Multivariable Multi-Model-based Magnetic Control System for the Current Ramp-up Phase in the National Spherical Torus Experiment (NSTX)

Wenyu Shi, Justin Barton, Majed Alsarheed and Eugenio Schuster

***Abstract*— By leveraging the availability of real time EFIT, we propose a robust, multi-model-based, multi-input-multi-output (MIMO) magnetic controller to provide current regulation, position stabilization, and shape control of the plasma during the current ramp-up phase in the National Spherical Torus Experiment (NSTX). During the ramp-up phase of the tokamak discharge, the magnetohydrodynamic (MHD) equilibrium continually evolves. As a consequence, the plasma response model obtained via linearization around the changing MHD equilibrium evolves as well. A robust controller is designed to stabilize this family of plasma models, which are reformulated into a nominal model with uncertainty. The proposed controller is composed of three loops: the first loop is devoted to plasma current regulation, the second loop is dedicated to plasma radial and vertical position stabilization, and the third loop is used to control the plasma shape and X-point location. A singular value decomposition (SVD) of the nominal plasma model is carried out to decouple and identify the most relevant control channels. The *DK*-iteration method, combining H_∞ synthesis and μ analysis, is applied to synthesize a closed-loop controller that minimizes the tracking errors and optimizes input efforts. Computer simulations illustrate the performance of the robust, multi-model-based, shape controller, showing potential for improving the performance of present non-model-based controllers.**

I. Introduction

The plasma shape requirements in a practical, highly-efficient tokamak are very stringent. The extreme shapes that must be achieved, the intrinsic instability in the plasma vertical position, the large number of control inputs and control outputs, the magnetohydrodynamic (MHD) equilibrium evolution, and the demanding regulation requirements make this problem very challenging.

The recent implementation of the real-time equilibrium reconstruction code rtEFIT [1] in the National Spherical Torus Experiment (NSTX) [2] allows the plasma to be shaped by controlling the magnetic flux at the plasma boundary. A non-model-based, single-input-single-output (SISO), PID-based shape controller that exploits this capability has been recently proposed [3]. Model-based control methods have been used in the past to design both vertical position [4] and shape controllers [5], [6] during the current flat-top phase. A PII controller containing a parallel connection of proportional, integral, and double integral gains has been applied in the design of controllers for the future ITER tokamak during the current ramp-up phase [7].

This work was supported by the NSF CAREER award program (ECCS-0645086), and US DOE DE-FG03-99ER54522.

Wenyu Shi (wenyu.shi@lehigh.edu), Justin Barton, Majed Alsarheed, and Eugenio Schuster are with the Department of Mechanical Engineering and Mechanics, Lehigh University, 19 Memorial Drive West, Bethlehem, PA 18015, USA.

The MHD equilibrium continually evolves during the ramp-up phase of the discharge. Twenty six scenario points are chosen to describe the plasma equilibrium evolution, which represent the prescribed reference trajectory of the system, during the plasma current ramp-up phase in NSTX. These 26 models are reformulated into a nominal model with uncertainty and singular value decomposition (SVD) is used to decouple and identify the most relevant control channels [8]. A robust controller based on the *DK*-iteration, combining H_∞ synthesis and μ analysis, is proposed to account for disturbances and uncertainties in the plasma model during the ramp-up phase of the discharge. The control goal is to drive the system to the reference plasma current, vertical and radial position, and shape.

This paper is organized as follows. In Section II, the NSTX tokamak is briefly described and the linearized plasma model is presented. In Section III, the design of the plasma control algorithm is described. Computer simulation results are presented in Section IV. Section V states the conclusions.

II. Description of NSTX

The system, which is composed of the plasma, shaping coils, and passive structure, is described using circuit equations derived for a particular plasma equilibrium from Faraday's Law and force balance relations in the radial and vertical directions. In addition, rigid radial and vertical displacements of the equilibrium current distribution are assumed, and a series of resistive plasma circuit equations are specified for the different equilibria [9]. The result is a series of circuit equations describing the linearized response, around a particular plasma equilibrium, of the conductor-plasma system to voltages applied to the active conductors. The poloidal cross section of NSTX, showing the distribution of active coils, is presented in Fig. 1. The linearized plasma response model is written in state space form

$$\dot{x}^p = Ax^p + Bu^p, \qquad \delta y^p = C\delta x^p, \tag{1}$$

with $x^p = [I_c^T\ I_v^T\ I_p^T]^T$ and $u^p = [V_c^T\ 0\ V_{no}^T]^T$, where I_c, I_v, and I_p represent the currents in the PF coils, vessel, and plasma respectively, V_c represents the vector of voltages applied to the PF coils, and V_{no} represents the effective voltage applied to drive plasma current by noninductive sources (no noninductive current source is considered in this work, i.e., $V_{no} = 0$). We define $\delta y^p = y^p - y^p_{eq}$ and $\delta x^p = x^p - x^p_{eq}$ where y^p_{eq} and x^p_{eq} are the values of the equilibrium outputs and states from which the model is derived. The output vector $y^p \in \Re^p$ $(p = 8)$ represents the fluxes ψ_1, ψ_2, ψ_3 at the control points, the magnetic field B_r and B_z at the desired

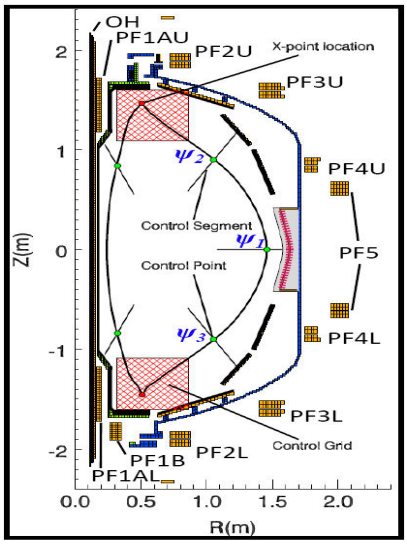

Fig. 1. NSTX Isoflux Control Configuration

X point location, the plasma radial and vertical positions R_p and Z_p (see Fig. 1), and the plasma current I_p.

During the plasma current ramp-up phase, the MHD equilibrium continually changes, and as a result, the plasma response model (1) changes. In this work, 26 scenario points from the experimental shot #124616 from 91 ms to 391 ms are chosen to describe the plasma equilibrium evolution.

III. Control System Design

A. Control System Structure

The proposed control architecture, shown in Fig. 2, is composed of three loops. The first loop, described in Section III-B, is devoted to plasma current regulation (PID controller). The second loop, described in Section III-C, is dedicated to plasma radial and vertical position stabilization (adaptive PID controller). The third loop, described in Section III-D, is used to control the plasma shape and X-point location (multi-input-multi-output (MIMO) robust controller).

B. Plasma Current Controller

The ohmic (OH) coil is used for plasma current regulation. The proposed plasma current controller is written as

$$V_{OH} = G_P^{I_p}\Delta I_p + G_I^{I_p}\int_0^t \Delta I_p dt + G_D^{I_p}\frac{d\Delta I_p}{dt}, \qquad (2)$$

where V_{OH} is the ohmic coil voltage, $\Delta I_p = I_p - I_P^{ref}$, and I_P^{ref} denotes the reference plasma current. The parameters $G_P^{I_p}$, $G_I^{I_p}$, and $G_D^{I_p}$ are the plasma current PID error gains.

C. Plasma Position Controller

Poloidal field coils PF2U/L, PF3U/L, and PF5 are used for plasma radial position control while poloidal field coils PF2U/L and PF3U/L are used for plasma vertical position control. Because the plasma response model (1) changes during the ramp-up phase, an adaptive PID controller is proposed to improve the tracking performance of the closed-loop system. In order to achieve this goal, an adjusted parameter k_c is introduced to the PID controller. In general, the goal is to minimize the closed-loop cost function $J_a(k_c) = e_a(k_c)^2/2$.

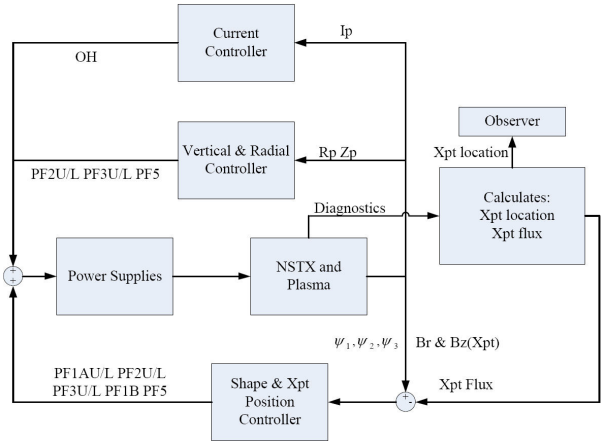

Fig. 2. NSTX Control System Architecture

The error e_a is defined as $e_a(k_c,t) = r_a(t) - y_a(k_c,t)$, where $r_a(t)$ is the reference and $y_a(k_c,t)$ is the system output, which will be defined below as the actual radial and vertical positions of the plasma. In order to make J_a small, it is reasonable to change k_c in the direction of the negative gradient of J_a, which is defined as

$$\dot{k}_c = \frac{dk_c}{dt} = -\lambda\frac{\partial J_a}{\partial k_c} = -\lambda\frac{\partial J_a}{\partial e_a}\frac{\partial e_a}{\partial k_c} = \lambda e_a\frac{\partial y_a}{\partial k_c}, \qquad (3)$$

where λ is the step length, and $\partial y_a/\partial k_c$ is the sensitivity derivative. The output is expressed as $y_a = P_a u_a$, where P_a is the transfer function of the system and the input u_a is defined as $u_a = k_c K_{PID} e_a$ where K_{PID} represents the PID controller transfer function. The goal is to make $y_a(k_c,t) = r_a(t)$ by choosing the optimal value of the adjusted parameter k_c, which is denoted k_c^*. The optimal reference is assumed to be $r_a = P_a k_c^* K_{PID} e_a = (k_c^*/k_c)P_a k_c K_{PID} e_a = (k_c^*/k_c)y_a$ [10]. The adjusted parameter k_c is therefore expressed as

$$\dot{k}_c = \lambda e_a\frac{\partial y_a}{\partial k_c} = \lambda e_a\frac{\partial\frac{(r_a k_c)}{k_c^*}}{\partial k_c} = \frac{\lambda}{k_c^*}e_a r_a = \nu e_a r_a, \qquad (4)$$

where ν is the adaptive gain. Using (4), the proposed radial position controller is then written as

$$\Delta V_{PF2_R}^{U/L} = \Delta V_{PF3_R}^{U/L} = \Delta V_{PF5_R} = V_{R_p} \qquad (5)$$

$$V_{R_p} = k_{cr}(G_P^{R_p}\Delta R_P + G_I^{R_p}\int_0^t \Delta R_P dt + G_D^{R_p}\frac{d\Delta R_P}{dt}) \qquad (6)$$

where $\Delta V_{PFi_R}^{(U/L)}$ represents the voltage contributed by the radial position controller to the PFi(U/L) coil ($i = 2,3,5$), $\Delta R_p = R_p - R_P^{ref}$, R_P^{ref} denotes the reference plasma radial position, $\dot{k}_{cr} = \nu_r \Delta R_p R_P^{ref}$ denotes the radial adjusted parameter, and ν_r denotes the radial adaptive gain. The parameters $G_P^{R_p}$, $G_I^{R_p}$, $G_D^{R_p}$ are the plasma radial position PID error gains. The proposed vertical position controller is written as

$$\Delta V_{PF2_Z}^{j} = \Delta V_{PF3_Z}^{j} = V_{Z_p}(j) \qquad (7)$$

$$V_{Z_p}(j) = (-1)^j k_{cz}(G_P^{Z_p}\Delta Z_P + G_I^{Z_p}\int_0^t \Delta Z_P + G_D^{Z_p}\frac{d\Delta Z_P}{dt}) \qquad (8)$$

where the superscript $j \in 0,1$ refers to upper (U) and lower (L) PF coils respectively, $\Delta V_{PFi_Z}^{(U/L)}$ represents the voltage contributed by the vertical position controller to the PFi(U/L) coil ($i = 2,3$), $\Delta Z_p = Z_p - Z_P^{ref}$, Z_P^{ref} denotes the reference

plasma vertical position, $\dot{k}_{cz} = \nu_z \Delta Z_p Z_P^{ref}$ denotes the vertical adjusted parameter, ν_z denotes the vertical adaptive gain. The parameters $G_P^{Z_p}$, $G_I^{Z_p}$, and $G_D^{Z_p}$ are the plasma vertical position PID error gains.

D. Plasma Shape and X-point Location Controller

The separate design of the plasma current and position controllers transforms the shape control problem into an output tracking problem. The tracking error is defined as $e(t) = r(t) - y(t)$, where the system output $y(t)$ is defined as the magnetic flux at three control points (Fig. 1) and the magnetic field components at the desired X-point location, i.e., $y = [\psi_1 \ \psi_2 \ \psi_3 \ B_r \ B_z]^T$ and $r(t)$ is the desired reference trajectory. The system input is defined as $u = [\Delta V^U_{PF1_S} \Delta V^U_{PF2_S} \Delta V^U_{PF3_S} \Delta V_{PF5_S} \Delta V^L_{PF3_S} \Delta V^L_{PF2_S} \Delta V^L_{PF1_S} \Delta V_{PF1B_S}]^T$, where $\Delta V^{(U/L)}_{PFi(B)_S}$ represents the voltage contributed by the shape controller to the $PFi(B)$(U/L) coil ($i = 1,2,3,5$). The control goal is to guarantee closed-loop stability while minimizing a quadratic cost function that weights the tracking error. The plasma shape and X-point location control algorithm is summarized by the following steps: (1) calculate ψ_1, ψ_2 and ψ_3 at the control points, and B_r and B_z at the desired X-point location; (2) estimate the actual X-point location and compute the flux at this point which is defined as ψ_{ref}; (3) make the flux at the control points track the flux ψ_{ref} and make B_r and B_z at the desired X-point location go to zero.

The relation between the inputs and the outputs is the linear model (1) which is expressed in terms of its transfer function $P(s) = Y(s)/U(s) = C(sI - A)^{-1}B$, where s denotes the Laplace variable and $Y(s)$ and $U(s)$ denote the Laplace transform of output and input vectors respectively. Assuming a constant reference $\bar{r}$ and closed-loop stabilization, the system will reach steady state as $t \to \infty$. It is possible then to define $\bar{y} = lim_{t\to\infty} y(t)$, $\bar{u} = lim_{t\to\infty} u(t)$, and $\bar{e} = lim_{t\to\infty} e(t) = \bar{r} - \bar{y}$. By invoking the final value theorem, we can express the closed-loop system in steady state as

$$\bar{y} = \bar{P}\bar{u} = -CA^{-1}B\bar{u} \qquad \bar{u} = \bar{\hat{K}}\bar{e} = \bar{\hat{K}}(\bar{r} - \bar{y}), \tag{9}$$

where $\hat{K}(s)$ represents the transfer function of the controller and $\bar{\hat{K}} = \hat{K}(0)$.

We consider the problem of minimizing a steady-state cost function given by

$$\bar{J} = \lim_{t\to\infty} e^T(t) Q e(t) = \bar{e}^T Q \bar{e} \tag{10}$$

where $Q \in \Re^{p\times p}$ is a symmetric positive definite weighting matrix and p is the number of outputs. In order to weight the control effort, another positive definite weighting matrix $R \in \Re^{m\times m}$ is also introduced where m is the number of inputs. We then define the "weighted" steady-state transfer function, and its singular value decomposition (SVD), as

$$\tilde{P} = Q^{1/2}\bar{P}R^{-1/2} = USV^T, \tag{11}$$

where $S = \mathrm{diag}(\sigma_1, \sigma_2, \cdots, \sigma_m) \in \Re^{m\times m}$, $U \in \Re^{p\times m}$ ($U^TU = I$), and $V \in \Re^{m\times m}$ ($V^TV = VV^T = I$). The steady-state input-output relation is now expressed as

$$\bar{y} = Q^{-1/2}\tilde{P}R^{1/2}\bar{u} = Q^{-1/2}USV^TR^{1/2}\bar{u}. \tag{12}$$

By invoking the properties of the SVD, we note that the columns of the matrix $Q^{-1/2}US$ define a basis for the subspace of obtainable steady-state output values. Therefore, we can always write

$$\bar{y} = Q^{-1/2}US\bar{y}^* \iff \bar{y}^* = S^{-1}U^TQ^{1/2}\bar{y} \tag{13}$$

where $\bar{y}^* \in \Re^m$. This implies that we will only be able to track the component of the reference vector $\bar{r}$ that lies in this subspace. We now write the reference vector as the sum of trackable components $\bar{r}_t$ and non-trackable components $\bar{r}_{nt}$, i.e., $\bar{r} = \bar{r}_t + \bar{r}_{nt}$, where

$$\bar{r}_t = Q^{-1/2}US\bar{r}^* \iff \bar{r}^* = S^{-1}U^TQ^{1/2}\bar{r} \tag{14}$$

with $\bar{r}^* \in \Re^m$ and $S^{-1}U^TQ^{1/2}\bar{r}_{nt} = 0$. By defining $\bar{u}^* = V^TR^{1/2}\bar{u}$, the relationship between $\bar{y}^*$ and $\bar{u}^*$ is obtained by using (12) as

$$\bar{y}^* = S^{-1}U^TQ^{1/2}\bar{y} = S^{-1}U^TQ^{1/2}Q^{-1/2}USV^TR^{1/2}\bar{u} = \bar{u}^* \tag{15}$$

and a one-to-one relationship between the inputs and outputs is obtained, and the new system is a square decoupled system. The steady state error is now written as

$$\bar{e} = \bar{r} - \bar{y} = Q^{-1/2}US(\bar{r}^* - \bar{y}^*). \tag{16}$$

Substituting this expression into (10), the performance index is expressed as

$$\bar{J} = (\bar{r}^* - \bar{y}^*)^T S^2 (\bar{r}^* - \bar{y}^*) = \sum_{i=1}^{m} \sigma_i^2 (\bar{r}_i^* - \bar{y}_i^*)^2. \tag{17}$$

The goal of the shape controller is to minimize the performance index $\bar{J}$. However, it is usually the case where $\sigma_1 > \cdots \sigma_k \gg \sigma_{k+1} > \cdots > \sigma_m > 0$. Note that the singular value σ_i, for $i = 1, \ldots, m$, is the weight parameter for the i^{th} component of the tracking error. Therefore, it is possible that with the intent of minimizing $\bar{J}$ in (17) we will spend a lot of control effort to minimize the i^{th} component of the tracking error, for $i > k$, which has a very small contribution to the overall value of the cost function. To avoid spending a lot of control effort for a marginal improvement of the cost function value, we partition the singular value set into significant singular values S_s and negligible singular values S_n. We then write

$$U = \begin{bmatrix} U_s & U_n \end{bmatrix}, V = \begin{bmatrix} V_s & V_n \end{bmatrix}, S = \begin{bmatrix} S_s & 0 \\ 0 & S_n \end{bmatrix} \tag{18}$$

to obtain a reduced form of the cost function defined in (17)

$$\bar{J}_s = \sum_{i=1}^{k} \sigma_i^2 (\bar{r}_i^* - \bar{y}_i^*)^2 = (\bar{r}_s^* - \bar{y}_s^*)^T S_s^2 (\bar{r}_s^* - \bar{y}_s^*) \tag{19}$$

where $\bar{r}_s^* = S_s^{-1}U_s^TQ^{1/2}\bar{r}$, $\bar{y}_s^* = S_s^{-1}U_s^TQ^{1/2}\bar{y}$, and $\bar{u}_s^* = V_s^TR^{1/2}\bar{u}$.

E. Design of μ Synthesis Controller

A frequency response study for the family of 26 decoupled plasma models obtained for the current ramp-up phase shows that the models do not have a large difference in magnitude, as shown in Fig. 3. Based on this frequency response study, the linear model at 115 ms, which is denoted as P_{top}, has the highest magnitude over the frequency range considered, and the model at 391 ms, which is denoted as P_{bottom}, has

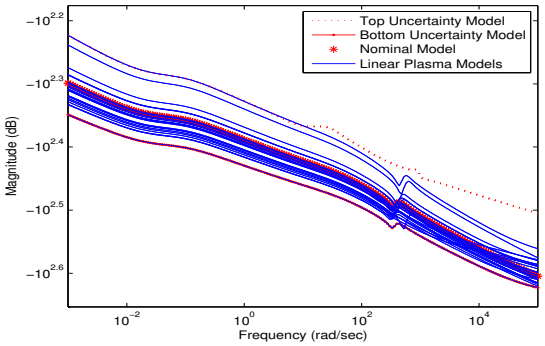

Fig. 3. Frequency Study of Plasma Models

the lowest magnitude. The model at 211 ms, which has the mean magnitude, is chosen as the nominal model, denoted as P_0. The family of plasma models can be considered as a one time-varying state-space model, which is written as an uncertain state-space model and formulated into a robust control framework.

By defining the matrix

$$M = \begin{bmatrix} A & B \\ C & D \end{bmatrix} \tag{20}$$

the transfer function of a linear system with state-space matrices A, B, C, and D can be written as an upper linear fractional transformation (LFT) [11], denoted by F_u, as

$$P(s) = F_u\left(M, \frac{1}{s}I\right) = C(sI - A)^{-1}B + D. \tag{21}$$

By defining the matrices

$$M_0 = \begin{bmatrix} A_0 & B_0 \\ C_0 & D_0 \end{bmatrix}, \Delta_i = \begin{bmatrix} \Delta A_i & \Delta B_i \\ \Delta C_i & \Delta D_i \end{bmatrix} \tag{22}$$

where $\Delta A_i = A_i - A_0$, $\Delta B_i = B_i - B_0$, $\Delta C_i = C_i - C_0$, $\Delta D_i = D_i - D_0$, and $i \in 1,2$ refers to the top and bottom models respectively, the state-space system matrices are now written as uncertain matrices as

$$\begin{aligned} A &= A_0 + \sum_{i=1}^{2} \delta_i \Delta A_i \quad B = B_0 + \sum_{i=1}^{2} \delta_i \Delta B_i \\ C &= C_0 + \sum_{i=1}^{2} \delta_i \Delta C_i \quad D = D_0 + \sum_{i=1}^{2} \delta_i \Delta D_i. \end{aligned} \tag{23}$$

By conducting a frequency analysis of the uncertain model of the system (23), the uncertain model is proven to capture the behavior of the family of reduced order decoupled plasma models as shown in Fig. 3.

The uncertainty can be formulated into a LFT by achieving the smallest possible number of repeated blocks by employing the method outlined in [12]. Thus, the matrix ΔM_i is formed as

$$\Delta M_i = \begin{bmatrix} \Delta A_i & \Delta B_i \\ \Delta C_i & \Delta D_i \end{bmatrix}. \tag{24}$$

By using singular value decomposition and grouping terms, the matrix ΔM_i is expressed as

$$\Delta M_i = U_i \Sigma_i V_i^T = (U_i \sqrt{\Sigma})(\sqrt{\Sigma} V_i^T) = \begin{bmatrix} L_i \\ W_i \end{bmatrix} \begin{bmatrix} R_i \\ Z_i \end{bmatrix}^T. \tag{25}$$

By employing (25), the uncertainty is written as

$$\delta_i \Delta M_i = \begin{bmatrix} L_i \\ W_i \end{bmatrix} \begin{bmatrix} \delta_i I_{q_i} \end{bmatrix} \begin{bmatrix} R_i \\ Z_i \end{bmatrix}^T \tag{26}$$

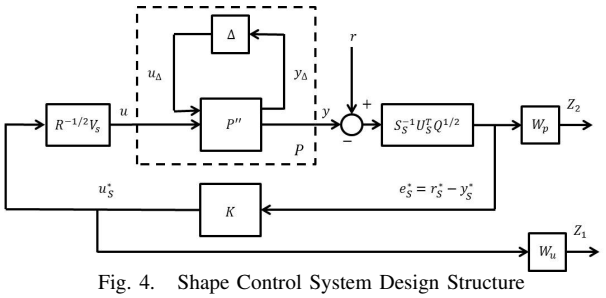

Fig. 4. Shape Control System Design Structure

where q_i is the rank of the matrix ΔM_i. The matrix M, defined in (20), is finally expressed as

$$M = M_0 + \sum_{i=1}^{2} \delta_i \Delta M_i = H_{11} + H_{12}\Delta H_{21} \tag{27}$$

where

$$\begin{aligned} H_{11} &= \begin{bmatrix} A_0 & B_0 \\ C_0 & D_0 \end{bmatrix} \qquad H_{12} = \begin{bmatrix} L_1 & L_2 \\ W_1 & W_2 \end{bmatrix} \\ H_{21} &= \begin{bmatrix} R_1^T & Z_1^T \\ R_2^T & Z_2^T \end{bmatrix} \qquad \Delta = \begin{bmatrix} \delta_1 I_{q_1} & 0 \\ 0 & \delta_2 I_{q_2} \end{bmatrix}. \end{aligned} \tag{28}$$

The representation of the matrix M, defined in (27), is equal to a lower LFT, denoted by F_l and written as

$$M = F_l(H, \Delta) = H_{11} + H_{12}\Delta H_{21} \tag{29}$$

where $H = \begin{bmatrix} H_{11} & H_{12} \\ H_{21} & 0 \end{bmatrix}$. Using (21) and (29), the transfer function $P(s)$ between the output y and the input u is next expressed as

$$\begin{aligned} P(s) &= F_u\left(F_l(H, \Delta), \frac{1}{s}I\right) = F_l\left(F_u\left(H, \frac{1}{s}I\right), \Delta\right) \\ &= F_l(P', \Delta) = F_u(P'', \Delta) \end{aligned} \tag{30}$$

where $P' = \begin{bmatrix} P''_{22} & P''_{21} \\ P''_{12} & P''_{11} \end{bmatrix}$ and $P'' = \begin{bmatrix} P''_{11} & P''_{12} \\ P''_{21} & P''_{22} \end{bmatrix}$. Using the partition of the generalized plant P'', the input/output equations are

$$y_\Delta = P''_{11}u_\Delta + P''_{12}u, \quad y = P''_{21}u_\Delta + P''_{22}u.$$

The control goal is to design a $k \times k$ feedback controller K, where k is the number of significant singular values defined in (18), that can stabilize the system and keep the tracking error $e_s^* = r_s^* - y_s^*$ small. The corresponding block diagram of the system is shown in Fig. 4 where the weight functions $W_p(s)$ and $W_u(s)$ are parameterized as

$$W_p(s) = K_p\left(\frac{\frac{s}{M_1} + w_{b1}}{s + w_{b1}A_1}\right)^2, W_u(s) = K_u\left(\frac{s + w_{b2}A_2}{\frac{s}{M_2} + w_{b2}}\right)^2$$

and the coefficients M_i, A_i, w_{bi}, for $i \in 1,2$, as well as K_p and K_u, are design parameters defined based on frequency-domain specifications.

The feedback system is now expressed in the conventional $\Delta - P^* - K$ robust control framework, where Δ is the uncertainty, P^* is the generalized plant, K is the feedback controller, $Z_1 = W_u u_s^*$, and $Z_2 = W_p e_s^*$. The input/output equations of the generalized plant P^* are expressed as

$$\begin{bmatrix} y_\Delta \\ Z_1 \\ Z_2 \\ e_s^* \end{bmatrix} = P^*(s) \begin{bmatrix} u_\Delta \\ r_s^* \\ u_s^* \end{bmatrix} = \begin{bmatrix} P^*_{11} & P^*_{12} & P^*_{13} \\ P^*_{21} & P^*_{22} & P^*_{23} \\ P^*_{31} & P^*_{32} & P^*_{33} \\ P^*_{41} & P^*_{42} & P^*_{43} \end{bmatrix} \begin{bmatrix} u_\Delta \\ r_s^* \\ u_s^* \end{bmatrix} \tag{31}$$

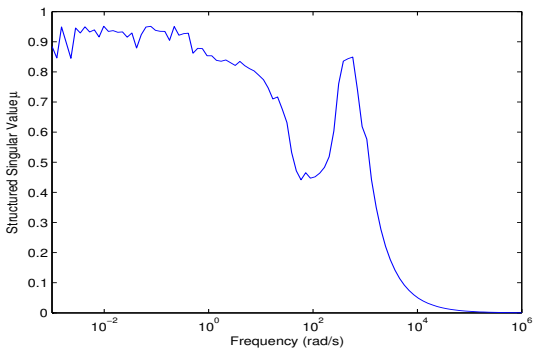

Fig. 5. Structured Singular Value μ versus Frequency

where $P_{11}^* = P_{11}''$, $P_{12}^* = 0$, $P_{13}^* = P_{12}'' R^{-1/2} V_s$, $P_{21}^* = 0$, $P_{22}^* = 0$, $P_{23}^* = W_u$, $P_{31}^* = -W_p S_s^{-1} U_s^T Q^{1/2} P_{21}''$, $P_{32}^* = W_p$, $P_{33}^* = -W_p S_s^{-1} U_s^T Q^{1/2} P_{22}'' R^{-1/2} V_s$, $P_{41}^* = -S_s^{-1} U_s^T Q^{1/2} P_{21}''$, $P_{42}^* = 1$, $P_{43}^* = -S_s^{-1} U_s^T Q^{1/2} P_{22}'' R^{-1/2} V_s$.

The closed-loop transfer function from the external input r_s^* to the external outputs $\begin{bmatrix} Z_1^T & Z_2^T \end{bmatrix}^T$ is defined as

$$T_{zr} = F_u(N, \Delta), \tag{32}$$

where $N = F_l(P^*, K)$. We seek a controller $K(s)$ that robustly stabilizes the system and minimizes the H_∞ norm of the transfer function $T_{zr}(N,\Delta)$, i.e.,

$$\min_{K(s)} \|T_{zr}(N,\Delta)\|_\infty = \min_{K(s)} (\sup_\omega \bar{\sigma}[T_{zr}(N,\Delta)(j\omega)]) \tag{33}$$

where $\bar{\sigma}$ represents the maximum singular value. The control method employed in this work to achieve the control goal (33) is the μ synthesis design technique [12].

There is no direct method to synthesize a μ-optimal controller, however the DK-iteration method, which combines H_∞ synthesis and μ analysis, can be used to obtain an iterative solution. This method starts with an upper bound on μ in terms of the scaled singular value $\mu(N) \leq \min(\bar{\sigma}(DND^{-1})$. Then, we seek a controller that minimizes the peak value over frequency of this upper bound

$$\min_K (\min \left\| DN(K)D^{-1} \right\|_\infty).$$

The controller is designed by alternating between the two minimization problems until reasonable performance is achieved. The DK-iteration steps are summarized as follows: (1) K step: Synthesize an H_∞ controller for the scaled problem, $\min_K \left\| DN(K)D^{-1} \right\|_\infty$ with fixed $D(s)$. (2) D step: Find $D(j\omega)$ to minimize $\bar{\sigma}(DND^{-1}(j\omega))$ at each frequency with fixed N. (3) Fit the magnitude of each element of $D(j\omega)$ to a stable and minimum-phase transfer function $D(s)$ and go to step 1. The iteration continues until $\left\| DN(K)D^{-1} \right\|_\infty < 1$ or the H_∞ norm no longer decreases.

To validate the designed controller, the robust stability of the closed-loop system is determined. The system is written in the $N-\Delta$ structure, and the robust stability is determined by evaluating the structured singular value

$$\mu(N_{11}(j\omega)) = \frac{1}{\min\{k_m | \det(I - k_m N_{11}\Delta) = 0\}} \tag{34}$$

where N_{11} is the transfer function from the input u_Δ to the output y_Δ. The closed-loop system is robustly stable for all allowable perturbations if and only if $\mu(N_{11}(j\omega)) < 1, \forall \omega$. Fig. 5 shows a plot of the structured singular value μ versus frequency, and as can be seen $\mu < 1$ for all frequencies. Therefore, the closed-loop system is robustly stable. In other words, the controller stabilizes the whole family of models.

Finally, the overall plasma shape and X-point location controller is written as

$$\hat{K}(s) = \frac{U(s)}{E(s)} = R^{-1/2} V_s K(s) S_s^{-1} U_s^T Q^{1/2} \tag{35}$$

where $E(s)$ denotes the Laplace transform of $e(t)$. The contribution to the coil voltages by the shape and X-point location controller is written as

$$\begin{aligned} V_{Shape} &= [\Delta V_{PF1A_s}^{U/L} \Delta V_{PF1B_s} \Delta V_{PF2_s}^{U/L} \Delta V_{PF3_s}^{U/L} \Delta V_{PF5_s}]^T \\ &= \mathscr{L}^{-1}\{\hat{K}(s)E(s)\} \end{aligned} \tag{36}$$

where $\mathscr{L}^{-1}$ denotes the inverse Laplace transform.

IV. Simulation Results

The simulation model is updated every 12 ms, and the reference values for the radial position, vertical position, plasma current and X-point location are those of the equilibrium around which the linearized model is obtained. The reference value for the flux at the control points is equal to the flux at the X-point, which is computed every 4 ms.

The parameters for the plasma current, vertical position and radial position loops are $G_P^{I_p} = 1$, $G_I^{I_p} = 0.02$, $G_D^{I_p} = 0.1$, $G_P^{R_p} = 800$, $G_I^{R_p} = 100$, $G_D^{R_p} = 1$, $\nu_r = 5$, $G_P^{Z_p} = 200$, $G_I^{Z_p} = 0$, $G_D^{Z_p} = 10$, $\nu_z = -10$. The weight matrices Q and R are set as $Q = \text{diag}\begin{bmatrix} 2 & 2 & 2 & 1 & 1 \end{bmatrix}$ and $R = \text{diag}\begin{bmatrix} 10 & 1.5 & 2.5 & 1 & 2.5 & 1.5 & 10 & 10 \end{bmatrix}$. The parameters for the μ synthesis are $M_1 = 100$, $w_{b1} = 0.01$, $A_1 = 7500$, $K_1 = 1000$, $M_2 = 500$, $w_{b2} = 1$, $A_2 = 75$, $K_2 = 0.001$.

The time responses for the plasma radial and vertical positions are shown in Fig. 6 (a). The radial and vertical positions are stabilized by the controller and the reference values are quickly achieved. Fig. 6 (b) (top) shows the time evolution of the plasma current, and the tracking error is less than 0.5%. The components of magnetic field at the desired X-point are shown in the Fig. 6 (b) (bottom), and the errors are less than 0.02 T. Fig. 6 (c) (top) shows both the flux at the X-point and the flux at the three control points (ψ_1, ψ_2, and ψ_3), and the flux at the control points tracks the flux at the X-point. Fig. 6 (c) (bottom) shows the tracking errors, which are less than 0.05 Wb. A series of four plasma boundary shapes at different times are shown in the Fig. 7. The blue circles represent the control points, the blue asterisk represents the actual location of the X-point, and the red asterisk represents the reference location of the X-point. The voltages of the PF coils are regulated according to the robust control law (35) in order to keep the plasma boundary at the control points and to regulate the X-point location around its desired value.

Based on the simulation, the control scheme proves to be successful in stabilizing the plasma position while regulating the plasma current and keeping the plasma shape and X-point location as specified. Because the controller forces the outputs to follow the desired reference trajectories, the MHD equilibrium evolves as specified during the ramp-up phase.

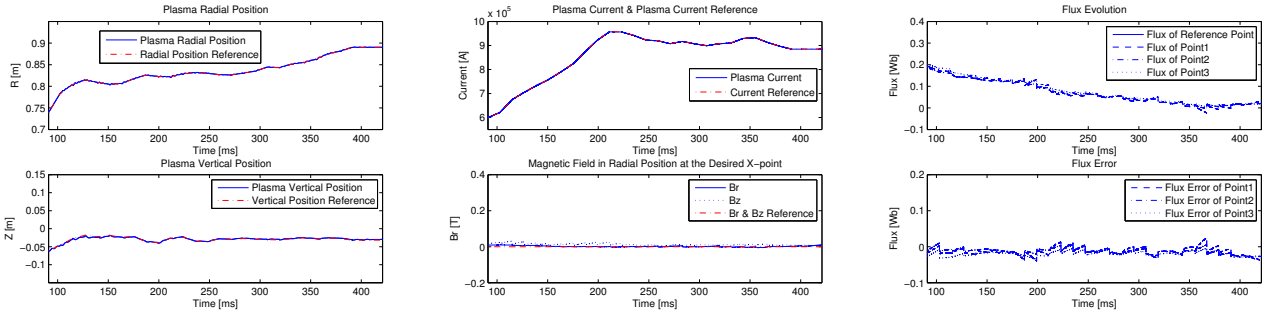

Fig. 6. (a) Plasma radial and vertical position; (b) Plasma current and magnetic field; (c) Magnetic flux & flux error at the control points.

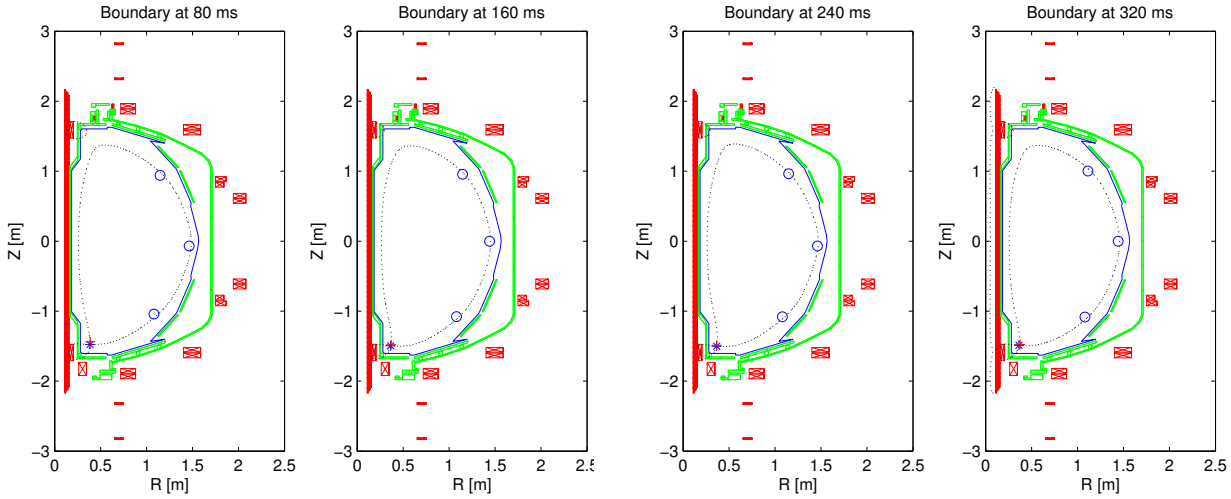

Fig. 7. Plasma Boundary at 80 ms, 160 ms, 240 ms and 320 ms

V. Conclusion

A robust multi-model-based MIMO controller was designed for NSTX. The design was based on linearized plasma response models in the current ramp-up phase. The availability of independent current and position controllers transforms the shape control problem into an output tracking problem. Singular value decomposition of the steady state transfer function is used to decouple the system and identify the most relevant control channels, and the shape controller is designed using this decoupled system. The DK-iteration technique, combining H_∞ synthesis and μ analysis, is used to minimize the tracking error and optimize input effort. The proposed controller was tested in simulations, and shows potential for expanding present experimental control capabilities. A more exhaustive and realistic simulation study is part of our future work before experimental validation. Ideally this study should include free-boundary simulations, real-time boundary reconstruction, synthetic noise in the measurements and disturbances.

VI. Acknowledgment

The authors would like to thank Michael Walker, Jim Leuer and David Humphreys from General Atomics and David Gates and Egemen Kolemen from Princeton Plasma Physics Laboratory for assisting us in building and validating the plasma response models.

References

[1] J. Ferron *et al.*, "Real Time Equilibrium Reconstruction for Tokamak Discharge Control," *Nuclear Fusion*, vol. 38, pp. 1055–1066, 1998.

[2] J. Chrzanowshi, C. Nenmeyer *et al.*, "National Spherical Torus Experiment (NSTX) Torus Design, Fabrication, and Assembly," in *Proceeding of the 18th Symposium on Fusion Engineering*, 1999.

[3] D. Gates *et al.*, "Plasma Shape Control on the National Spherical Torus Experiment (NSTX) Using Real-time Equilibrium Reconstruction," *Nuclear Fusion*, vol. 46, pp. 17–23, 2006.

[4] Y. Mitrishkin, V. Dokuka *et al.*, "Plasma Magnetic Robust Control in Tokamak Reactor," in *Proceeding of the 45th IEEE Conference on Decision and Control*, 2006.

[5] D. Humphreys, M. Walker *et al.*, "Initial Implementation of a Multivariable Plasma Shape and Position Controller on the DIII-D Tokamak," in *Proceeding of the 2000 IEEE International Conference on Control Applications*, 2000.

[6] M. Ariola, G. Ambrosino *et al.*, "Design and Experimental Testing of a Robust Multivariable Controller on a Tokamak," *IEEE Transactions on Control Systems Technology*, vol. 10, no. 5, pp. 646–653, 2002.

[7] Y. Mitrishkin, A. Korostelev *et al.*, "Design and Modeling of ITER Plasma Magnetic Control System in Plasma Current Ramp-up Phase on DINA Code," in *Proceeding of the 49th IEEE Conference on Decision and Control*, 2009.

[8] G. Ambrosino *et al.*, "Design and Implementation of an Output Regulation Controller for the JET Tokamak," *IEEE Transactions on Control Systems Technology*, vol. 16, no. 6, pp. 1101–1111, 2008.

[9] M. Walker and D. Humphreys, "Valid Coordinate Systems for Linearized Plasma Shape Response Models in Tokamaks," *Fusion Science and Technology*, vol. 50, no. 4, pp. 473–489, 2006.

[10] K. Astrom and B. Wittenmark, *Adaptive Control*. Dover Publications, Inc. Mineola, New York, 2008.

[11] S. Skogestad and I. Postlethwaite, *Multivariable Feedback Control Analysis and Design*. John Wiley & Sons, Ltd, 2005.

[12] A. Packard, "What News with μ: Structured Uncertainty in Multivariable Control," Ph.D. dissertation, UC Berkeley, 1988.